# Chapter 4: Turbulence at Small Scales

# Part 7: Analysis of Kolmogorov spectra

## (1) 1D Dissipation spectra

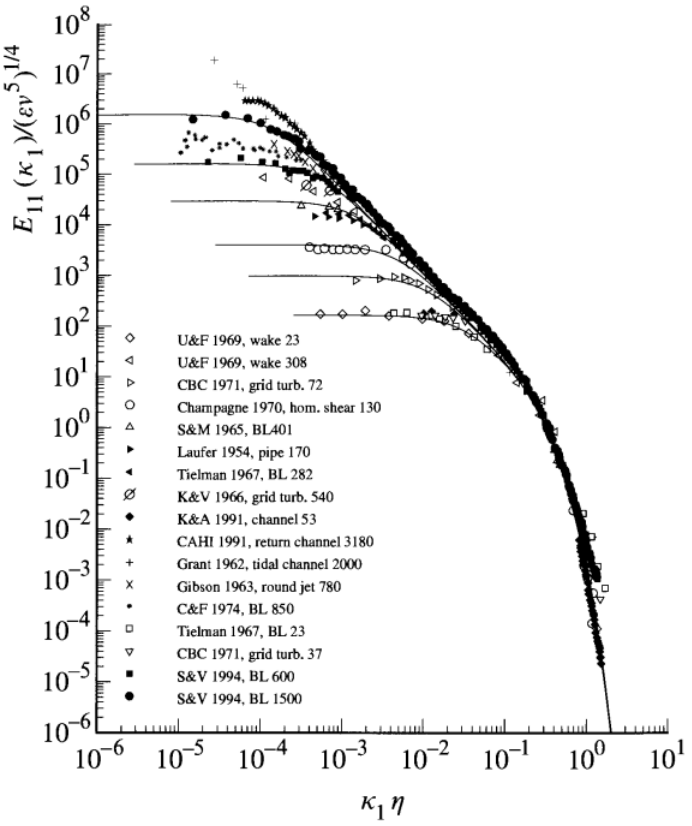


Fig. 6.14. Measurements of one-dimensional longitudinal velocity spectra (symbols), and model spectra (Eq. (6.246)) for $R_\lambda = 30, 70, 130, 300, 600$, and 1,500 (lines). The experimental data are taken from Saddoughi and Veeravalli (1994) where references to the various experiments are given. For each experiment, the final number in the key is the value of $R_\lambda$.

Scaled Kolmogorov spectrum log-log plot[1]: $\varphi_{11}(\kappa_1\eta) = E_{11}(\kappa_1)/(\varepsilon\nu^5)^{1/4}$ vs. $\kappa_1\eta$

Universal $f(\kappa_1\eta)$ for high Re and for $\kappa_1 > \kappa_{EI}$: universal equilibrium range.

Data lie on a single curve for $\kappa_1\eta > 0.1$: exponential decay.

Power law for $\kappa_1\eta < 0.1$ and extent of region increases with $R_\lambda$: inertial subrange $(\kappa_1\eta)^{-5/3}$.

The model spectrum is accurate.

[1] See Chapter 4 Part 4 for universal equilibrium and inertial subrange scaling.

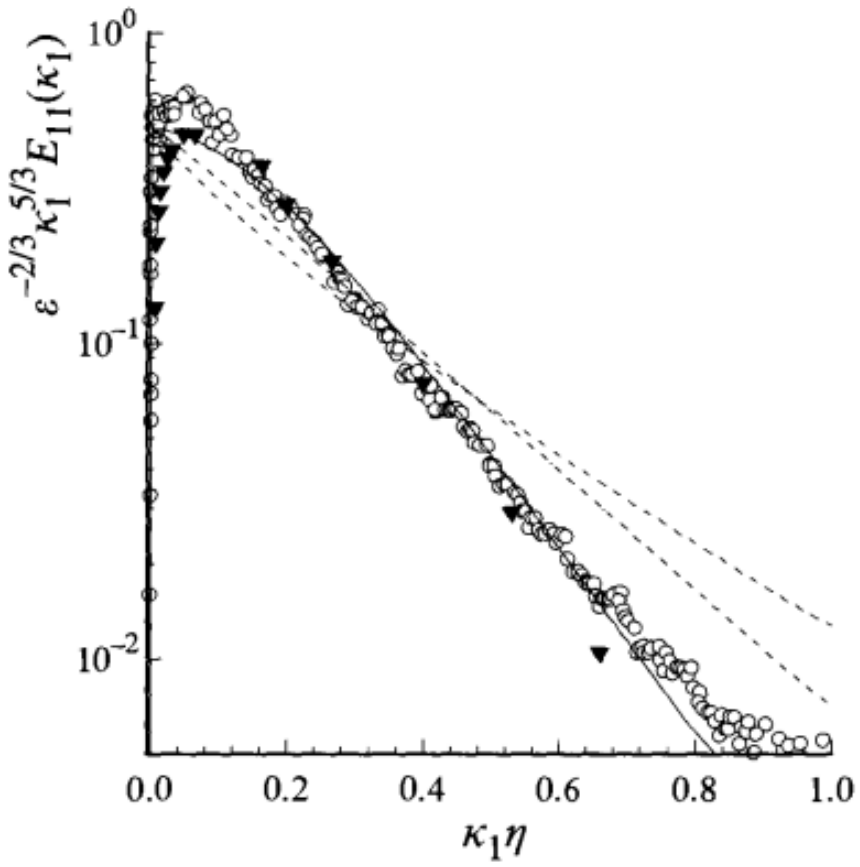


Fig. 6.15. Compensated one-dimensional velocity spectra. Measurements of Comte-Bellot and Corrsin (1971) in grid turbulence at $R_\lambda \approx 60$ (triangles), and of Saddoughi and Veeravalli (1994) in a turbulent boundary layer at $R_\lambda \approx 600$ (circles). Solid line, model spectrum Eq. (6.246) for $R_\lambda = 600$; dashed line, exponential spectrum Eq. (6.253); dot–dashed line, Pao's spectrum, Eq. (6.254).

Scaled compensated spectrum log-linear plot[2]: $\Psi_{11} = E_{11}(\kappa_1)\varepsilon^{-2/3}{\kappa_1}^{5/3}$ vs. $\kappa_1\eta$

Emphasizes dissipation range.

For $\kappa_1\eta > 0.1$, agreement different flows support universality of large $\kappa$ spectra.

Straight line behavior for $\kappa_1\eta > 0.3$ indicates exponential decay for highest $\kappa$.

Model spectrum represents the data accurately.

[2] A log–linear (sometimes log–lin) plot has the logarithmic scale on the y-axis, and a linear scale on the x-axis; a linear–log (sometimes lin–log) is the opposite. The naming is output–input (y–x), the opposite order from (x, y).

Alternative models for $f_\eta(\kappa\eta)$ (Pope Ex. 6.33):

$$f_\eta(\kappa\eta) = \exp(-\beta_0\kappa\eta)$$

$$f_\eta(\kappa\eta) = \exp\left[-\frac{3}{2}C(\kappa\eta)^{4/3}\right]$$

Not as good as model spectrum.

**3D Dissipative spectrum**

$$\varepsilon = 2\,\upsilon\int_0^\infty \kappa^2 E(\kappa,t)d\kappa \quad (\mathrm{m^2/s^3})$$

$$D(\kappa) = 2\nu\kappa^2 E(\kappa) \quad (\mathrm{m^2/s \times m^{-2} \times m^3/s^2 = m^3/s^3})$$

Cumulative dissipation

$$\varepsilon_{(0,\kappa)} \equiv \int_0^\kappa D(\kappa')d\kappa'$$

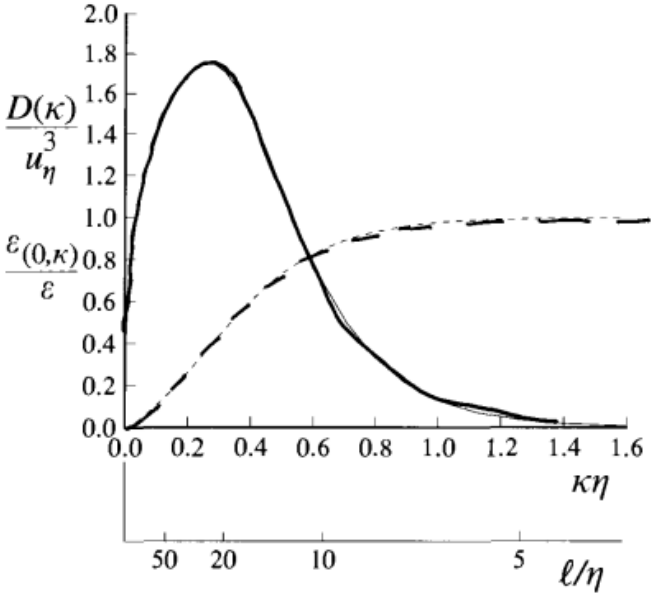


Fig. 6.16. The dissipation spectrum (solid line) and cumulative dissipation (dashed line) corresponding to the model spectrum Eq. (6.246) for $R_\lambda = 600$. $\ell = 2\pi/\kappa$ is the wavelength corresponding to wavenumber $\kappa$.

Table 6.1. *Characteristic wavenumbers and lengthscales of the dissipation spectrum (based on the model spectrum Eq. (6.246) at* $R_\lambda = 600$)

| Defining wavenumbers | $\kappa\eta$ | $\ell/\eta$ |
|---|---|---|
| Peak of dissipation spectrum | 0.26 | 24 |
| $\varepsilon_{(0,\kappa)} = 0.1\varepsilon$ | 0.10 | 63 |
| $\varepsilon_{(0,\kappa)} = 0.5\varepsilon$ | 0.34 | 18 |
| $\varepsilon_{(0,\kappa)} = 0.9\varepsilon$ | 0.73 | 8.6 |

Peak of dissipation spectrum $\kappa\eta \approx 0.26$, corresponding to $l/\eta \approx 24$, while the centroid (where $\varepsilon_{(0,\kappa)} = \frac{1}{2}\varepsilon$) occurs at $\kappa\eta \approx 0.34$, corresponding to $l/\eta \approx 18$.

Thus, most of $\varepsilon$ occurs for $0.1 < \kappa\eta < 0.75$, or $60 > l/\eta > 8$ which is $> \eta$.

Therefore, dissipative motions scale with $\eta$, but are not equal to $\eta$. The boundary between the inertial subrange and the dissipation range is taken to be $l_{DI} = 60\eta$.

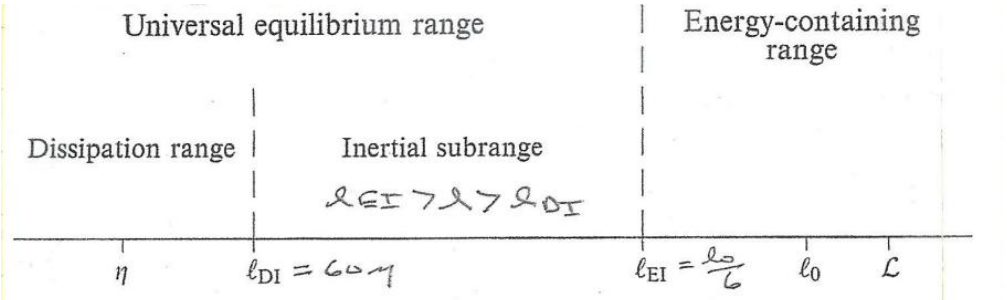


Fig. 6.1. Eddy sizes $\ell$ (on a logarithmic scale) at very high Reynolds number, showing the various lengthscales and ranges.

## (2) 1D Spectra Inertial Subrange[3]

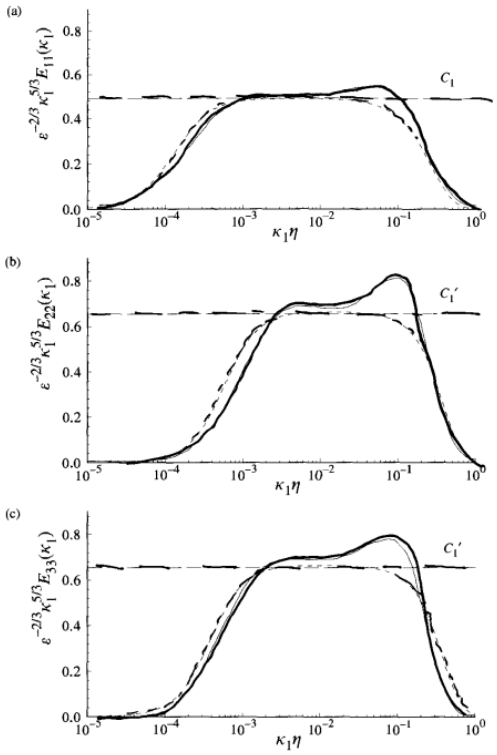


$$\frac{18}{55}C = 0.49$$

$$\frac{4}{3}C_1 = 0.65$$

Fig. 6.17. Compensated one-dimensional spectra measured in a turbulent boundary layer at $R_\lambda \approx 1{,}450$. Solid lines, experimental data Saddoughi and Veeravalli (1994); dashed lines, model spectra from Eq. (6.246); long dashed lines, $C_1$ and $C_1'$ corresponding to Kolmogorov inertial-range spectra. (For $E_{11}$, $E_{22}$ and $E_{33}$ the model spectra are for $R_\lambda = 1{,}450$, 690, and 910, respectively, corresponding to the measured values of $\langle u_1^2\rangle$, $\langle u_2^2\rangle$, and $\langle u_3^2\rangle$.)

Second Kolmogorov hypothesis predicts a -5/3 spectrum in the inertial subrange, which is best examined using a linear-log compensated spectrum plot.

$$\Psi_{11} = E_{11}(\kappa_1)/\varepsilon^{2/3}{\kappa_1}^{-5/3} = C_1 = 0.49$$

Data is within 20% of the predicted value over two decades of $\kappa$, over which range of ${\kappa_1}^{5/3}$ increases by a factor of 2000.

$$\kappa_1\eta = 10^{-3} \rightarrow (\kappa_1\eta)^{5/3} = 10^{-5}$$

$$\kappa_1\eta = 10^{-1} \rightarrow (\kappa_1\eta)^{5/3} = 2.2 \cdot 10^{-2}$$

$$\rightarrow 2.2 \cdot 10^{-2}/10^{-5} \sim 2000$$

For $\kappa_1\eta > 2 \times 10^{-3}$, $E_{22} \cong E_{33}$, i.e., "locally" isotropic behavior.

[3] Also see discussion Chapter 4, Part 6, pg.18.

### (3) 3D Spectra energy-containing range

Examination of $E(\kappa)$ in the energy containing range unlike universal equilibrium range is a function of flow at hand.

$E(\kappa)$ is better than $E_{11}(\kappa_1)$ since $E_{11}(\kappa_1)$ only depends on $|\kappa| > \kappa_1$. $E(\kappa)$ is difficult to obtain from $E_{11}(\kappa_1)$ as requires differentiation: $E(\kappa) = \frac{1}{2}\kappa^3 \frac{d}{d\kappa}\left[\frac{1}{\kappa}\frac{dE_{11}}{d\kappa}\right]$.

Appropriate scales for normalization are the turbulent kinetic energy $k$ and $L_{11}$.

For isotropic turbulence:

$$k = \int_0^\infty E(\kappa)d\kappa$$

$$\int_0^\infty \frac{E(\kappa)}{\kappa}d\kappa = \frac{4}{3\pi}kL_{11} \quad \text{(Chapter 4 Part 5 A.8; k = } \frac{3}{2}\overline{u^2}\text{)}$$

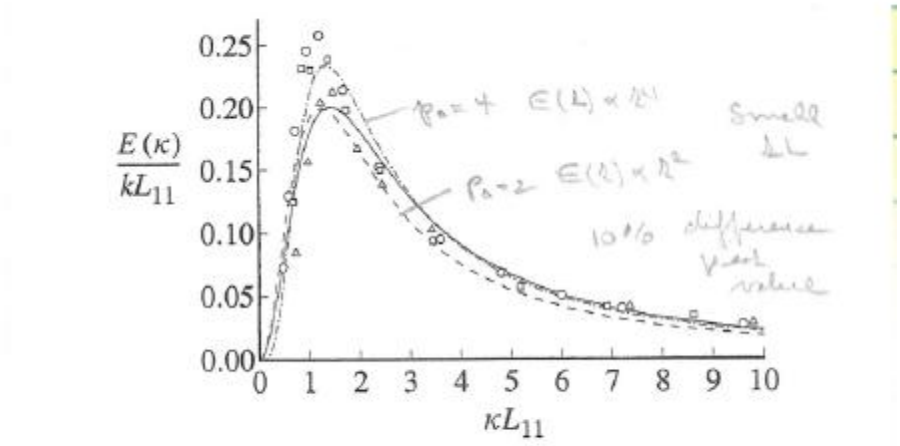


Fig. 6.18. The energy-spectrum function in isotropic turbulence normalized by $k$ and $L_{11}$. Symbols, grid-turbulence experiments of Comte-Bellot and Corrsin (1971): ○, $R_\lambda = 71$; □, $R_\lambda = 65$; △, $R_\lambda = 61$. Lines, model spectrum, Eq. (6.246): solid, $p_0 = 2$, $R_\lambda = 60$; dashed, $p_0 = 2$, $R_\lambda = 1{,}000$; dot–dashed $p_0 = 4$, $R_\lambda = 60$.

Model spectrum accurate and $\kappa L_{11}$ scaling small changes with Re. $p_0 = 4$ vs. 2 mainly affects small $\kappa L_{11}$ and show 10% difference peak value, which is likely within $U_D$. Note $p_0 = 2$ is used in model spectrum, although $p_0 = 4$ appears better overall fit the data.[4]

[4] See discussion Chapter 4 Part 6 pg. 4.

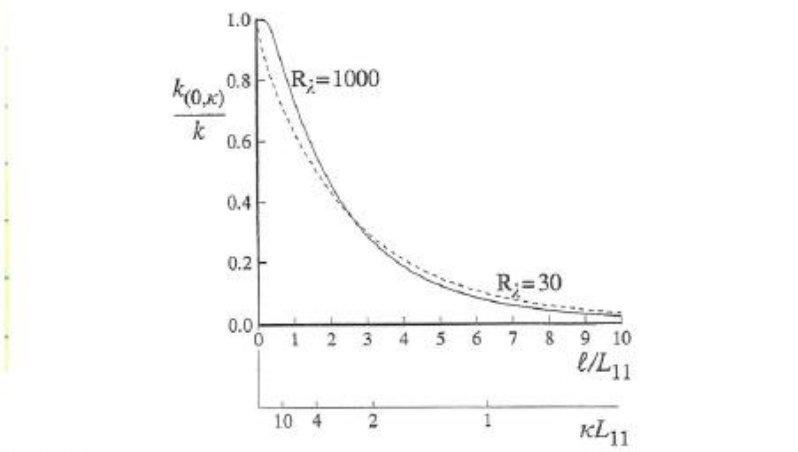


Fig. 6.19. The cumulative turbulent kinetic energy $k_{(0,\kappa)}$ against wavenumber $\kappa$ and wavelength $\ell = 2\pi/\kappa$ for the model spectrum.

The cumulative kinetic energy is given by: $k_{(0,\kappa)} = \int_0^\kappa E(\kappa')dk'$

Table 6.2. *Characteristic wavenumbers and lengthscales of the energy spectrum (based on the model spectrum Eq. (6.246) at* $R_\lambda = 600$*)*

| Defining wavenumber | $\kappa L_{11}$ | $\ell/L_{11}$ |
|---|---|---|
| Peak of energy spectrum | 1.3 | 5.0 |
| $k_{(0,\kappa)} = 0.1k$ | 1.0 | 6.1 |
| $k_{(0,\kappa)} = 0.5k$ | 3.9 | 1.6 |
| $k_{(0,\kappa)} = 0.8k$ | 15 | 0.42 |
| $k_{(0,\kappa)} = 0.9k$ | 38 | 0.16 |

The centroid of the spectrum is at $\kappa L_{11} \approx 4$ ($\frac{l}{L_{11}} \approx 1.5$ ) and 80% of the energy is contained in motions of length scale $\frac{1}{6}L_{11} < l < 6L_{11}$. On this basis Pope takes the length scales characterizing the energy-containing motions to be $l_0 = L_{11}$ and $l_{EI} = \frac{1}{6}L_{11}$. However, it will be shown later that $l_0 \approx 2L_{11}$ is a more appropriate choice such that $l_{EI} = \frac{1}{6}L_{11} = \frac{1}{12}\ l_0$.

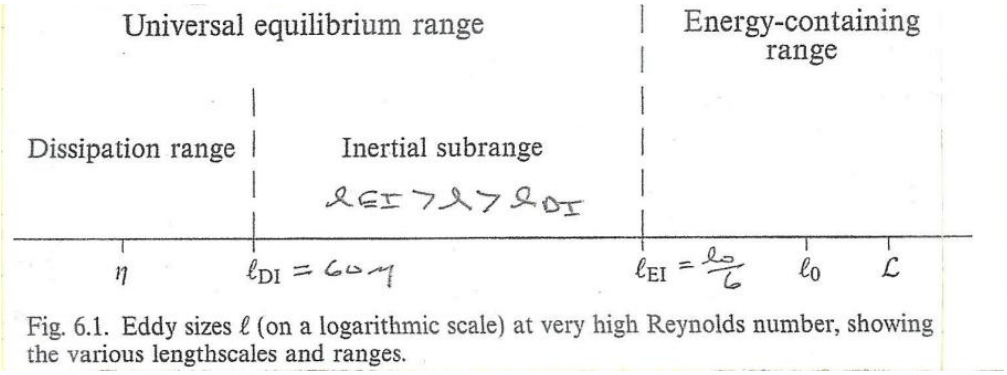


Fig. 6.1. Eddy sizes $\ell$ (on a logarithmic scale) at very high Reynolds number, showing the various lengthscales and ranges.

## (4) 3D Spectra Effects of the Reynolds number

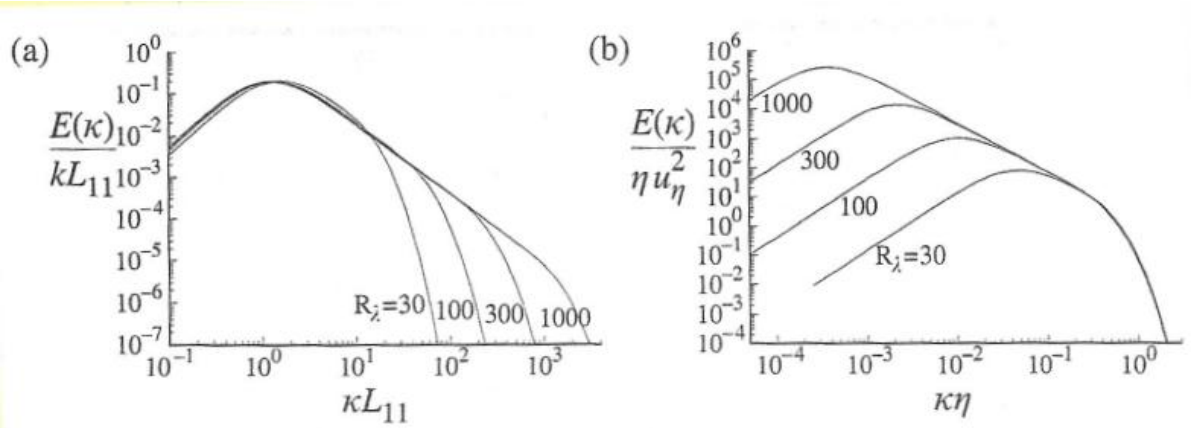


Fig. 6.20. The model spectrum for various Reynolds numbers, scaled by (a) $k$ and $L_{11}$, and (b) Kolmogorov scales.

(a): model spectrum normalized by $\kappa$ and $L_{11}$ for a range of Re shows that energy-containing ranges of the spectra $(0.1 < \kappa L_{11} < 10)$ are very similar, whereas for increasing $R_\lambda$, the extent of the -5/3 region increases, and the exponential decay region moves to higher values of $\kappa L_{11}$.

(b): same spectra normalized by $\kappa\eta$, shows dissipation ranges ($\kappa\eta > 0.1$) are very similar, whereas the -5/3 region and the energy range move to lower values of $\kappa\eta$ for increasing $R_\lambda$.

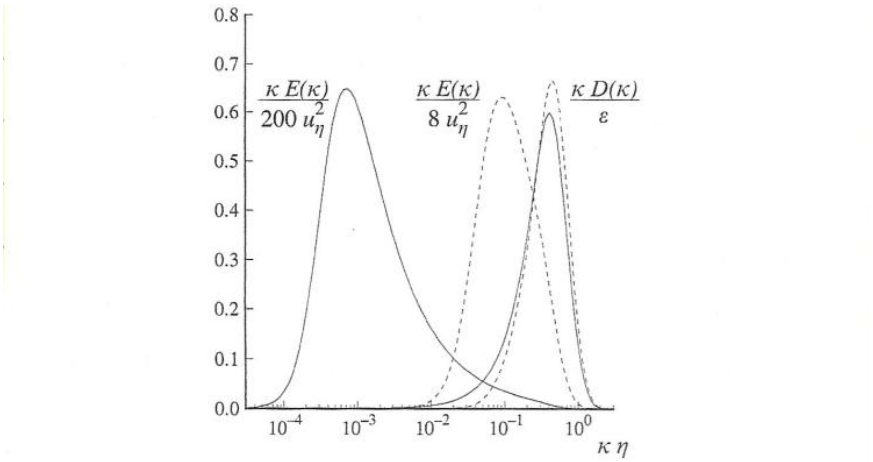


Fig. 6.21. Model energy and dissipation spectra normalized by the Kolmogorov scales at $R_\lambda = 1{,}000$ (solid lines) and $R_\lambda = 30$ (dashed lines). (Note the scaling of $E(\kappa)$.)

Contrast between high Re and low Re energy and dissipation spectra.

The energy in the wave number range $(\kappa_a, \kappa_b)$

$$k_{(\kappa_a,\kappa_b)} = \int_{\kappa_a}^{\kappa_b} E(\kappa)d\kappa = \int_{\kappa_a}^{\kappa_b} \kappa E(\kappa)d\ln\kappa$$

High Re spectrum contains more energy.

Low Re, energy and dissipation spectra overlap (no clear separation of scales), whereas for high Re there is a significant separation of scales.

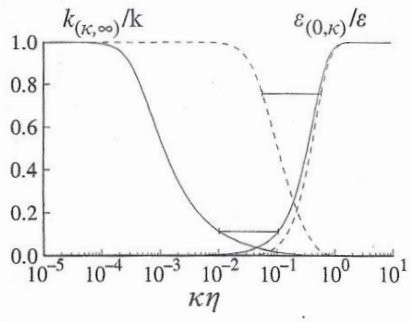


Fig. 6.22. The fraction of the energy at wavenumbers greater than $\kappa$ $(k_{(\kappa,\infty)}/k)$ and the fraction of the dissipation at wavenumbers less than $\kappa$ $(\varepsilon_{(0,\kappa)}/\varepsilon)$ for the model spectrum at $R_\lambda = 1{,}000$ (solid line) and at $R_\lambda = 30$ (dashed line). For the two Reynolds numbers, the horizontal bars identify the 'decade of wavenumbers of most overlap' between the energy and dissipation spectra.

Quantification of the overlap between the energy and dissipation spectra.

$k_{(\kappa,\infty)}/k =$ fraction of energy due to wave number $> \kappa$

$\varepsilon_{(0,\kappa)}/\varepsilon =$ fraction of dissipation due to wave number $< \kappa$

If there were a complete separation of scales then, with increasing $\kappa$, $k_{(\kappa,\infty)}/k$ would decrease to zero before $\varepsilon_{(0,\kappa)}/\varepsilon$ rises from zero.

For large $R_\lambda$ small overlap, but large overlap for small $R_\lambda$.

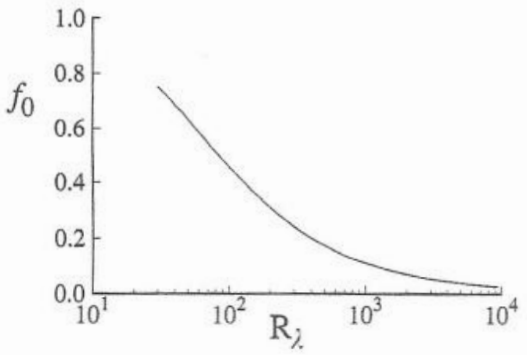


Fig. 6.23. The fraction $f_0$ of the energy and dissipation contributed by the wavenumber decade of maximum overlap as a function of $R_\lambda$ for the model spectrum.

Overlap fraction for decade of wavenumber $(\kappa_m, 10\kappa_m)$

$$f_0 = \frac{k_{(\kappa_m,\infty)}}{k} \Big/ \frac{\varepsilon((0,10\kappa_m))}{\varepsilon}$$

| $R_\lambda$ | 30 | 1000 |
|---|---|---|
| $f_0$ | 0.75 | 0.11 |

Very large $R_\lambda$ required for there to be a decade of wave numbers in which both energy and dissipation are negligible.

Energy cascade:

$$\varepsilon = \frac{u_0^3}{l_0}$$

Where $u_0$ and $l_0$ are characteristic velocity and length scales of energy containing eddies. Taking $u_0 = k^{1/2}$ and $l_0 = L_{11} \Rightarrow \varepsilon = k^{3/2}/L_{11}$ vs. using the definition $L \equiv k^{3/2}/\varepsilon$ (Chapter 4 Part 3 pg. 14; Pope pg. 200)

$$\varepsilon = \frac{k^{3/2}}{L} = \varepsilon = \frac{k^{3/2}}{L_{11}}\left(\frac{L_{11}}{L}\right) \Rightarrow \frac{L_{11}}{L} = 1$$

That is, scaling $\varepsilon = k^{3/2}/L_{11}$ is equivalent only if $\frac{L_{11}}{L} = 1$.

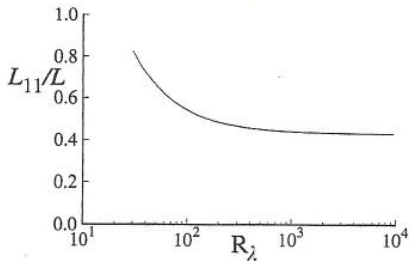


Fig. 6.24. The ratio of the longitudinal integral lengthscale $L_{11}$ to $L = k^{3/2}/\varepsilon$ as a function of the Reynolds number for the model spectrum.

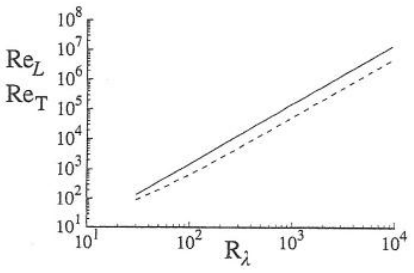


Fig. 6.25. Turbulence Reynolds numbers $Re_L$ (solid line) and $Re_T$ (dashed line) as functions of $R_\lambda$ for the model spectrum.

However, Fig. 6.24 shows that $L_{11}/L$ only approaches 1 for small $R_\lambda < 10^2$, which is the requirement for turbulent flow and $L_{11}/L \rightarrow 0.43$ as $R_\lambda$ increases. Therefore, for turbulent flow, $l_0 = L = \frac{k^{3/2}}{\varepsilon}$ is the proper definition of the length scale for large eddies.; and $L_{11} \approx l_0/2$ such that $l_{EI} = \frac{1}{6}L_{11} = \frac{1}{12}\ l_0$.

Fig. 6.25: Shows relation between different turbulent Reynolds numbers.

$$Re_L \equiv \frac{k^{1/2}L}{\nu} = \frac{k^2}{\varepsilon\nu} = \frac{3}{20}R_\lambda{}^2 \quad \text{(Chapter 4 Part 3 A.3)}$$

and

$$Re_T \equiv \frac{L_{11}u'}{\nu} = \sqrt{\frac{2}{3}}\frac{L_{11}}{L}Re_L \sim \frac{1}{20}R_\lambda{}^2$$

which is an alternate turbulent Re using $L_{11}$ and $u' = u_{rms} = \left[\frac{2}{3}k\right]^{1/2}$

In turbulent flows, Pope proposes (based geometric scales)

$$Re = \frac{U\mathcal{L}}{\nu} \sim 10 Re_T$$

$$\frac{u'}{U} \approx 0.2, \qquad \frac{L_{11}}{\mathcal{L}} = 0.5$$

$$R_\lambda \approx \sqrt{2Re}$$

However, considering $l_0 = L \sim 2L_{11}$, and $\mathcal{L}$ as the characteristic length scale of the flow (usually based on the geometry of the problem), it is more reasonable to estimate $\mathcal{L} \sim 6L_{11}$, since 80% of the flow energy is contained in motions of length scale $\frac{1}{6}L_{11} < l < 6L_{11}$, as discussed previously.

$$Re = \frac{U\mathcal{L}}{\nu} \sim \frac{u' 6L_{11}}{0.2\nu} \sim 30 Re_T$$

$$R_\lambda \approx \sqrt{\frac{2}{3}Re}$$

**(5) The shear-stress spectrum** (see Pope Ex. 6.35)

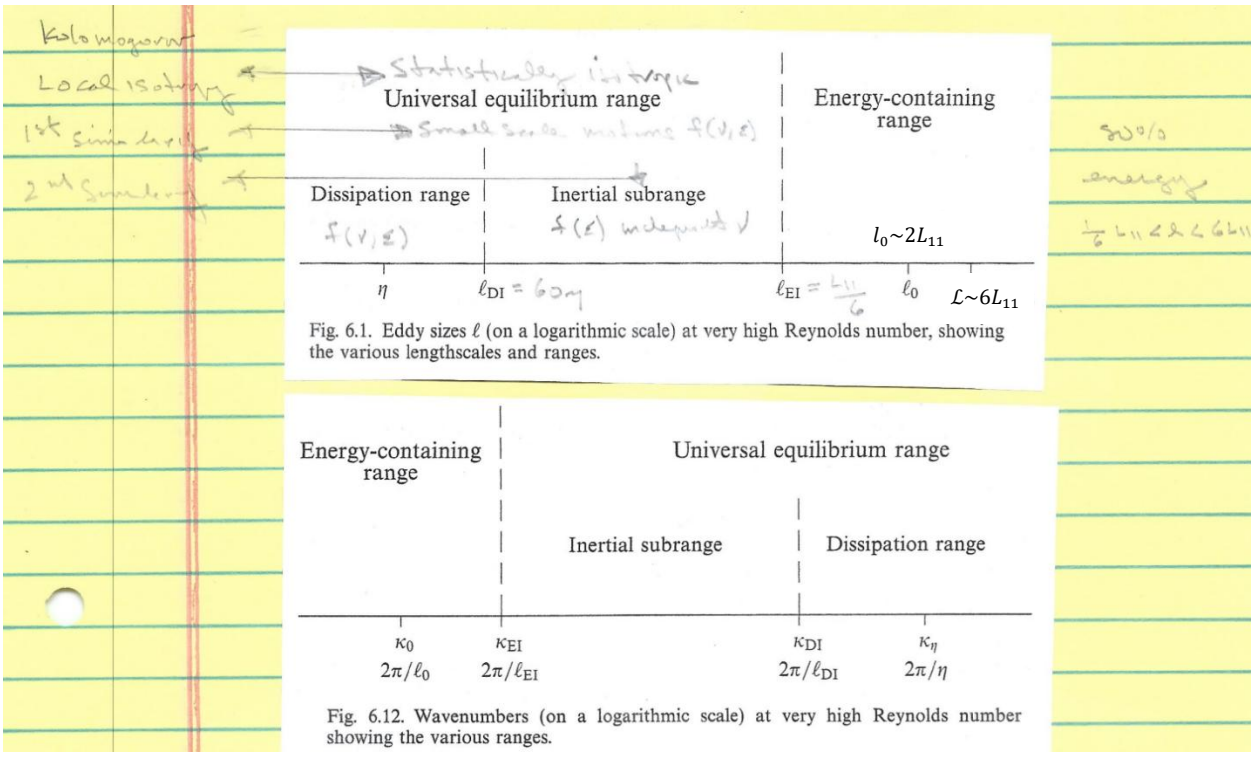


Fig. 6.1. Eddy sizes $\ell$ (on a logarithmic scale) at very high Reynolds number, showing the various lengthscales and ranges.

Fig. 6.12. Wavenumbers (on a logarithmic scale) at very high Reynolds number showing the various ranges.

Dissipation + inertial subrange: $E(\kappa) = \varepsilon^{2/3}\kappa^{-5/3}\Psi(\kappa\eta)$

Inertial subrange: $E(\kappa) = C\varepsilon^{2/3}\kappa^{-5/3}$

Dissipation range: $D(\kappa) = 2\nu\kappa^2 E(\kappa)$

Locally isotropic turbulence, i.e., isotropy only at small scales: $\overline{u_1 u_2} = 0$, $\mathcal{E}_{12}(\underline{\kappa}) = 0$, $E_{12}(\kappa_1) = 0$.

For simple shear flows, e.g., with $\mathcal{S} \equiv \frac{\partial \overline{U_1}}{\partial x_2} > 0 \ \left[\frac{1}{s}\right] \Rightarrow$ non-isotropic turbulence, e.g., homogeneous shear flow (Chapter 6 Part 3): Production $P = -\overline{u_1 u_2}\frac{\partial \overline{U_1}}{\partial x_2}$, $\alpha = \overline{u_1 u_2}/k \approx -0.3$, and $\frac{P}{\varepsilon} \approx 1$ such that $\mathcal{S}k/\varepsilon = \frac{P}{\alpha\varepsilon} \approx 3$. In view of the relation

$$\overline{u_1 u_2} = \int_0^\infty E_{12}(\kappa_1)\, d\kappa_1$$

$$\varepsilon = \frac{u_0^3}{l_0} \ \left[\frac{m^2}{s^3}\right]$$

$E_{12}(\kappa_1)$ must be anisotropic at least over part of the wave number range.

Therefore, it is important to determine the contributions to $\overline{u_1 u_2}$ from various scales of motion. The picture that emerges is that wave numbers in the energy containing range primarily contribute to $\overline{u_1 u_2}$ such that for higher wave numbers $E_{12}(\kappa_1)$ decays more rapidly than $E_{11}(\kappa_1)$, which is consistent with local isotropy.

$\tau =$ time scale (of motions of wavenumber $\kappa$) $=$ eddy turnover time.

$\mathcal{S}\tau =$ non-dimensional mean shear (rate of strain) characterizes influence $\mathcal{S}$, i.e., if small $\mathcal{S}\tau$ then level of anisotropy created by $\mathcal{S}$ is also small.

Dissipation range $\tau = \tau_\eta = (\nu/\varepsilon)^{1/2}$: $\mathcal{S}\tau_\eta \ll 1$ for local isotropy at $\kappa$

$$= 3{Re_L}^{-1/2}$$

$$= 9{R_\lambda}^{-1}$$

Which shows that a high Re is required.

Inertial sub range $\tau(\kappa) = (\kappa^2\varepsilon)^{-1/3}$ (formed from $\kappa$ and $\varepsilon$, as per Chapter 4 Part 0 pg. 8) and for local isotropy at $\kappa$

$$\mathcal{S}\tau(\kappa) = \mathcal{S}(\kappa^2\varepsilon)^{-1/3} \ll 1$$

with length scale (formed from $\varepsilon$ and $\mathcal{S}$) $L_\mathcal{S} \equiv \varepsilon^{\frac{1}{2}}\mathcal{S}^{-\frac{3}{2}} \approx L/6$ ( $L = k^{3/2}/\varepsilon$); thus, for local isotropy

$$(\kappa L_\mathcal{S})^{2/3} \approx \kappa L_\mathcal{S} \gg 1$$

Or equivalently

$$\mathcal{S}^{-1}(\kappa^2\varepsilon)^{1/3} \gg 1$$

$$L_\mathcal{S}\varepsilon^{-\frac{1}{2}} = \mathcal{S}^{-\frac{3}{2}}\,[m]$$

$$\mathcal{S} = L_\mathcal{S}^{-\frac{2}{3}}\varepsilon^{\frac{1}{3}}\left[\frac{1}{s}\right]$$

For high Re, ${L_\mathcal{S}}^{-1} \ll \kappa \ll \eta^{-1}$ for the wave number range within the inertial subrange wherein anisotropy for the present circumstances is only a small perturbation due $\mathcal{S}$ on background isotropy characterized by $f(\varepsilon)$. Therefore,

$$E_{12}(\kappa_1) = f(\kappa_1, \varepsilon, \mathcal{S}) \propto \mathcal{S} = L_\mathcal{S}^{-2/3}\varepsilon^{1/3}$$

and since small perturbation assumed linear $f(\mathcal{S})$. From dimensional analysis (note units $E_{12}$ are $m^3/s^2$)

$$\frac{E_{12}(\kappa_1)}{u_{\mathcal{S}}^2 L_{\mathcal{S}}} = \hat{E}_{12}(\kappa_1 L_{\mathcal{S}})$$ = nondimensional function

$u_{\mathcal{S}}$ = velocity scale (formed from $\varepsilon$ and $\mathcal{S}$) = $(\varepsilon/\mathcal{S})^{1/2} \approx k^{1/2}/2$

The linearity of $E_{12}$ with $\mathcal{S}$ determines $\hat{E}_{12}$:

$$\frac{E_{12}(\kappa_1)}{u_{\mathcal{S}}^2 L_{\mathcal{S}}} = -C_{12}(\kappa_1 L_{\mathcal{S}})^{-7/3}$$ or

$$E_{12}(\kappa_1) = -C_{12}\mathcal{S}\varepsilon^{1/3}{\kappa_1}^{-7/3}$$ where $C_{12}$ is a constant.

**Appendix A.1**

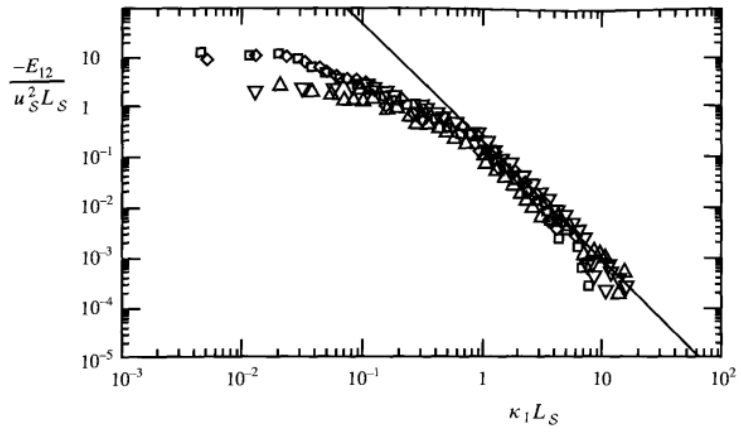


Fig. 6.26. Shear-stress spectra scaled by $u_{\mathcal{S}}$ and $L_{\mathcal{S}}$: line, Eq. (6.277) with $C_{12} = 0.15$; symbols, experimental data of Saddoughi and Veeravalli (1994) from turbulent boundary layers with $R_\lambda \approx 500$ to 1,450.

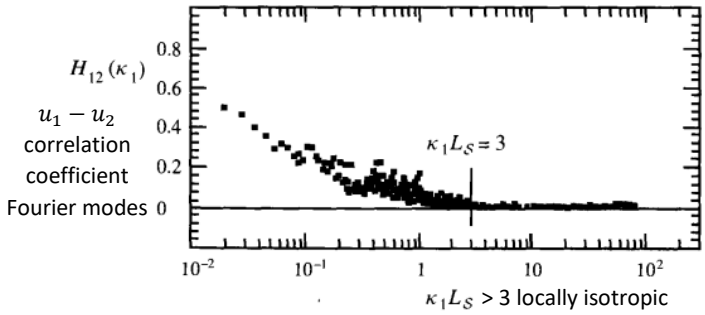


Fig. 6.27. The spectral coherency measured in a turbulent boundary layer at $R_\lambda = 1{,}400$ (Saddoughi and Veeravalli 1994).

Agrees data for $\kappa_1 L_{\mathcal{S}} > 0.5$ with $C_{12} = 0.15$.

Shows that $E_{12}(\kappa_1)$ decays more rapidly than $E_{11}(\kappa_1)$, i.e., $-7/3$ vs. $-5/3$, so that anisotropy decreases rapidly with $\kappa_1$.

Based on Fig. 6.27 it is proposed that

$$\kappa_1 L_{\mathcal{S}} > 3$$

for the locally isotropic region of the spectrum, which is consistent with $l_{EI} = L_{11}/6$ marking the start of the inertial sub range, since (with assumption, i.e., $L = L_{11}$)

$$(2\pi/l_{EI})\, L_{\mathcal{S}} \approx 6 \quad \text{vs.} \approx 12 \ (\text{for } L = 2L_{11})$$

Major conclusion: dominant contribution $\overline{u_1 u_2}$ is from $\kappa$ in the energy containing range, and at higher $\kappa, E_{12}(\kappa_1)$ decays more rapidly than $E_{11}(\kappa_1)$, which is consistent with local isotropy.

Another demonstration of the concept of Reynolds-number similarity at large Re is the contrast between the TKE and shear stress spectra. As seen in Figure 5.10, the shear stress spectrum decays more quickly than the energy spectrum, implying that the influence of large-scale anisotropy on small scales is minimal, especially in high-Re flows. In particular, at large frequencies, the shear stress spectrum is effectively zero, supporting the idea of local isotropy at small scales.

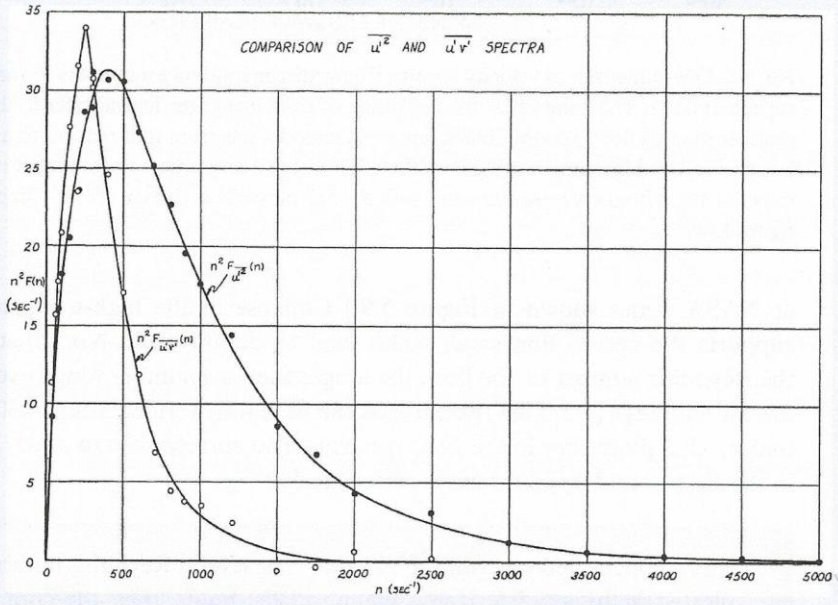


Fig. 5.10 The $\overline{u'^2}$ and $\overline{u'v'}$ frequency spectra from experimental channel measurements. (Image credit: Laufer (1950), figure 12)

## Appendix A

## A.1: $E_{12}$ dimensional analysis

$$E_{12}(\kappa_1) = f(\kappa_1, \varepsilon, \mathcal{S}) \propto \mathcal{S}$$

$$E_{12}(\kappa_1) = -C_{12}\, \mathcal{S} \kappa_1^{\alpha} \varepsilon^{\beta} \left[\frac{m^3}{s^2}\right]$$

$$C_{12}\ [-]$$

$$S\ \left[\frac{1}{s}\right]$$

$$\varepsilon\ \left[\frac{m^2}{s^3}\right]$$

$$\kappa_1\ \left[\frac{1}{m}\right]$$

By dimensional analysis:

$$\begin{cases} L: -\alpha + 2\beta = 3 \\ T: -1 - 3\beta = -2 \end{cases}$$

$$\begin{cases} \beta = \dfrac{1}{3} \\ -\alpha + \dfrac{2}{3} = 3 \rightarrow \alpha = -\dfrac{7}{3} \end{cases}$$

Therefore,

$$E_{12}(\kappa_1) = -C_{12} \mathcal{S} \varepsilon^{1/3} {\kappa_1}^{-7/3}$$